Proceedings of 15th IOE Graduate Conference
Peer Reviewed
Year: 2024 Month: May Volume: 15
ISSN: 2350-8914 (Online), 2350-8906 (Print)

Numerical Study and Comparison of Drag Coefficient of Sphere at Various Blockage Ratios

Hardik Shrestha [a], Rajesh Kumar Shrestha [b], Ashim Thapa [c], Binita Ale [d], Prabin Karki [e], Dipesh Karki [f]

[a, b, c, d, e, f] *Department of Mechanical and Automobile Engineering, Pashchimanchal Campus, IOE, Tribhuvan University, Nepal*

[a] sthahardik@gmail.com, [b] gemsraj246@gmail.com, [c] thapasim56@gmail.com, [d] ananyashrestha77@gmail.com, [e] prabinkarki220@gmail.com, [f] carkey.dpsh03@gmail.com

Abstract

The drag coefficient plays a dominant role in the motion of objects in fluid. The main objective of this project is to perform numerical analysis to obtain drag coefficient of sphere at various Reynold numbers. Furthermore, we also aim to see the effect of blockage ratio in the drag coefficient of the sphere. The geometry of the sphere is modelled in design modular and meshed in ICEM CFD to study the flow behavior around the sphere. The diameter of the sphere was set at 0.1m. The dimensions of the computational grid were changed accordingly to obtain the blockage ratio of 0.3 and 0.5. We have also visualized the pressure contour, velocity contour and flow separation. Additionally, this study compares the result obtained from Reynold Averaged Navier-Stokes (RANS) simulation with the existing literature and the subsonic wind tunnel. Additionally, the study compares simulation results with experimental data to validate the accuracy of numerical value. Overall, this analysis provides valuable insights into the flow characteristics around a sphere aiding in the design and optimization in the various engineering systems.

Keywords

Blockage ratio, Coefficient of drag, Drag, Sphere, ANSYS

1. Introduction

Drag is formally defined as the force corresponding to the rate of decrease in momentum in the direction of the undisturbed external flow around the body, this decrease being calculated between stations at infinite distances upstream and downstream of the body. Thus it is the total force or drag in the direction of the undisturbed flow. It is also the total force resisting the motion of the body through the surrounding fluid.

Skin- riction drag (or surface-friction drag): This is the drag that is generated by the resolved components of the traction due to the shear stresses acting on the surface of the body. This traction is due directly to viscosity and acts tangentially at all points on the surface of the body. At each point it has a component aligned with but opposing the undisturbed flow (i.e. opposite to the direction of flight). The total effect of these components, taken (i.e. integrated) over the whole exposed surface of the body, is the skin-friction drag. It could not exist in an inviscid flow. Form drag arises because of the shape of the object. The general size and shape of the body are the most important factors in form drag; bodies with a larger presented cross- section will have a higher drag than thinner bodies; sleek objects have lower form drag [1]. Thus, a form drag is the direct result of the turbulence form in the wake region. Parasitic drag is a combination of form drag and skin friction drag. Parasitic drag (profile drag) is a type of aerodynamic drag that acts on any object when the object is moving through a fluid regardless of the flow regime. The major contribution in total drag in a subsonic flow is the friction drag, which is largely dependent upon the wetted area, the surface smoothness of that area, and the presence of any discontinuities in the shape. Form drag is by far the main contribution to overall drag for bluff bodies like the cylinder, whereas for streamlined bodies skin-friction drag is predominant, form drag being less than 10% of overall drag. For bluff bodies even minimal streamlining can be very effective [2] The other two types of drag are: Pressure drag (which is generated by the resolved components of the forces due to pressure acting normal to the surface at all points) and wave drag (which caused by the shock wave).

The Reynolds number is used to classify the flow regime and to predict the behavior of the fluid. The force that a flowing fluid exerts on a body in the flow direction is called drag. Most of the time, it is an undesirable effect and we try to minimize it. A moving fluid exerts normal pressure force and tangential shear forces on the surface as drag forces. Tangential shear forces are due to no-slip condition caused by viscous effect. Both of these forces have components in the direction of flow, hence the drag force is due to combined effects of pressure and wall shear forces in the flow direction.

The study of drag in the sphere is crucial across a plethora of STEM disciplines. In sports like golf or tennis, understanding the drag on the ball can influence the design of equipment. Engineers may optimize the shape and surface properties of sports equipment to improve performance and accuracy. Drag analysis in a bluff body like sphere is relevant in space exploration for spacecraft re-entry. Extensive study has been done in the field of experimental and numerical analysis of drag in the sphere in various. The wake properties and vortex shedding of the sphere has been studied using various algorithms like finite volume analysis, finite element analysis, and spectral method.

One of the most notable and important study in the field of

flow over a sphere is that of Achenbach [3], in which flow past spheres in the Reynolds number at the range of 5×10^4 and 6×10^6 for a smooth surface was studied. Wieselberger [4] studied the flow over sphere which T. Maxworthy [5], had done experiments for Reynolds numbers between 2×10^5 and 6×10^6 by measuring the pressure distribution around the circle of longitude under a variety of conditions including the effect of the various boundary layer trip arrangements. These three experimental data are used in the current thesis in order to compare with the numerical results at the end of the current study. Wulf Armin; Akdag, Vedat [6] studied on a tuned grid generation with ICEM CFD package that supports multiblock structured, unstructured tetrahedral and unstructured hexahedral grids. Major development efforts have been spent to extend ICEM multiblock structured and hexahedral unstructured grid generation capabilities. The modules added were a parametric grid generation module and a semi-automatic hexahedral grid generation module. A fully automatic version of the hexahedral grid generation module for around a set of predefined objects in rectilinear enclosures have been developed.

Kravchenko & Moin [7] performed simulations of flow over cylinder using LES (Large eddy simulations) in the subcritical area with Re=3900 using structural grid type with finite volume method as their solution method for the filtered Navier-Stokes equations. Kravchenko and Moin, Parnaudeau et al. and Mani et al. used LES at $R_e = 3900$ using structured grid type and high order finite difference method.

Constantinescu [8] have also simulated the flow over a sphere at a Reynolds number of 1.0×10^4 using both LES and DES models and found that both methods gave essentially the same results. In The behavior of the flow past a sphere at varying Reynolds numbers has been studied by a number of researchers Taneda [9] used flow visualization methods to study the wake of a sting-mounted sphere for $5 < R_e < 300$, where R_e is the Reynolds number based on the sphere diameter D and velocity. He determined that separation from the rear of a sphere occurs at R_e 24 and results in the generation of an axisymmetric vortex ring.

Tomboulides [10] presents numerical results from a spectral element solution of the flow over a sphere for $25 < R_e < 10{,}000$ and with large-eddy simulation at Re 2000. He shows steady axisymmetric flow for R_e 212 with initial separation at R_e 20. He found a regular bifurcation, i.e. a transition to steady flow, at R_e of 212. The vorticity of the resulting steady flow field resembled the double-thread wake. Vojtěch Spálenský and etal. [11] studied the problems of CFD simulating airflow over a dimpled spherical surface and its validation by the wind tunnel testing. The low-cost simulation approach was applied to be run on a common PC using the commercial software ANSYS CFX. The wind tunnel testing had been performed in the laboratory of aerodynamics at the Department of Air Force and Aircraft Technology of the University of Defense. Measured results of the drag coefficient versus the Reynolds number for smooth and dimpled spheres were compared and discussed. Presented simulation corresponds adequately to the experimental results. It can be stated that the CFD simulation is suitable for simulating the flow over the dimpled surface and for the evaluation of the drag coefficient for smooth and dimpled spheres.

2. Methodology

Geometry was modeled in a design modular and computational domain was created for different blockage ratios. The turbulent viscous flow model was chosen as K-ω that provides better prediction near walls.Meshing was done in ICEM CFD meshing where blocking, O-grid generation, Edge meshing and Face meshing was done as per required. The mesh quality was evaluated by ensuring desired format, and is further processed for solution in ANSYS Fluent. The mesh independence test was done to assess the impact of mesh resolution in the simulation results. After mesh refinement, and Drag force and Drag coefficient was calculated with convergence criteria of 0.001. Different results were calculated by varying the Reynolds number and blockage ratio.

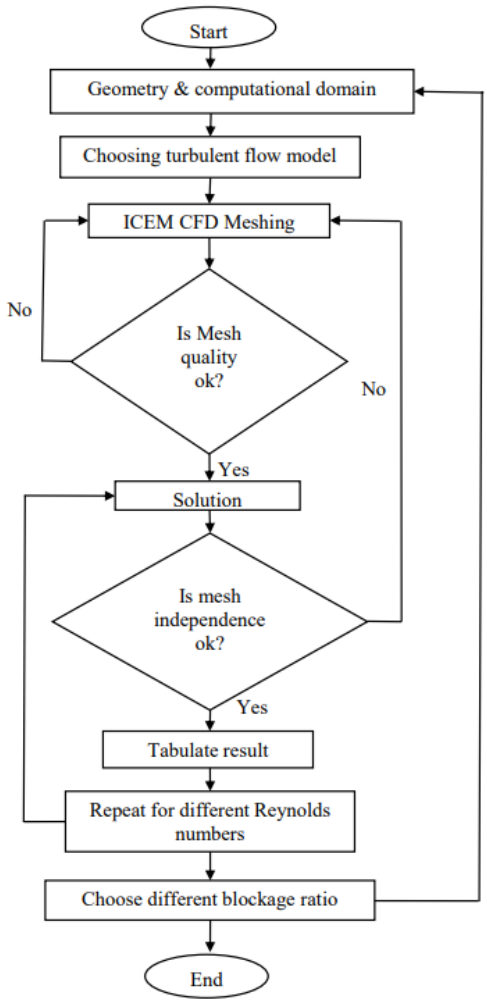

Figure 1: Methodological Diagram

Turbulent flows are characterized by a large range of vertical structures at different scales, both in time and space, which interact with each other and exchange energy. The largest scales contain most of the kinetic energy for the flow. As larger structures are broken into smaller ones, this energy is transferred to progressively smaller scales. RANS stands for Reynolds-Averaged Navier-Stokes equations. An averaging operation can be applied to the Navier-Stokes equations to obtain the mean equations of fluid flows called Reynolds

Averaged Navier-Stokes (RANS) equations. These are very similar to the original equations but contains some additional terms in the momentum equations called Reynolds stress terms that are unknown and need to be modelled. The other two model for turbulence modeling are the direct numerical simulation and large eddy simulation. The computational cost requirement for the latter two are high. Thus, RANS model of resolving the turbulence is chosen for the current work

$$\rho \overline{u}_j \frac{\partial \overline{u}_i}{\partial x_j} = \rho \overline{f}_i + \frac{\partial}{\partial x_j}\left(-\overline{p}\delta_{ij} + \mu\left(\frac{\partial \overline{u}_i}{\partial x_j} + \frac{\partial \overline{u}_j}{\partial x_i}\right) - \rho \overline{u}_i \overline{u}_j\right) \quad (1)$$

Multiple RANS models are offered by ANSYS Fluent. SST-K ω is chosen for our work. Since evaluating drag requires near wall modelling of the flow, SST k ω is best suited for the purpose. It is a hybrid model combining the Wilcox k-ω and the k-ϵ models. A blending function activates the Wilcox model near the wall and the k-ϵ model in the free stream. It is a two-equation model. That means in addition to the conservation equations, it solves two transport equations (PDEs), which the k-ϵ model in the free stream. It is a two-equation model. That means in addition to the conservation equations, it solves two transport equations (PDEs), which account for the history effects like convection and diffusion of turbulent energy. The two transported variables are turbulent kinetic energy (k),which determines the energy in turbulence, and specific turbulent dissipation rate(ω) which determines the rate dissipation per unit turbulent kinetic energy.

2.1 Computational Domain

The computational domain was created in design modular for different blockage ratios. Blockage ratio is defined as the ratio of diameter of the sphere to the diameter of the computational domain .i.e. In all the blockage ratio the length of the computational domain in the upstream of the sphere (L) was fixed at 10D and the length downstream of the sphere was fixed 20.

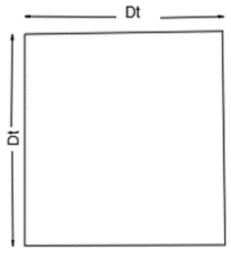

Figure 2: Side view of Compuatational domain

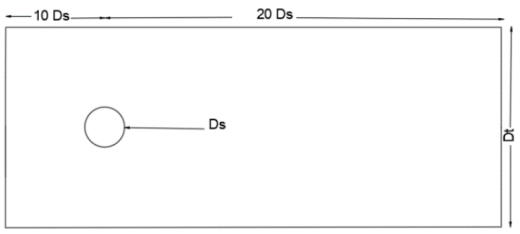

Figure 3: Front view of Compuatational domain

2.2 Mesh Generation

The set was imported in ICEM CFD to generate the hex meshing. Hexahedral elements typically require fewer elements to represent a given geometry accurately compared to tetrahedral elements. This can lead to reduced mesh size, resulting in faster solution times and lower computational resource requirements. Hex (or quad) meshes generally work better for wall-bounded flows since we can maintain orthogonal grids in the wall- normal direction. This is a consequence of the better accuracy of the hex elements since the angle between faces can be kept close to 90°. When the Reynolds number is high, we need very fine spacing in the wall-normal direction. Hex grids allow very fine wall-normal spacing but without large face skewness Appropriate name was given to the computational domain i.e. inlet, walls and outlet; the domain was defined as FLUID. Then blocking was initiated from using a split edge tool. The domain was split such that the sphere was enclosed in a cube. Index control was used to isolate the cube and the sphere. The blocking strategy for this sphere cube geometry involves creating an O-Grid around the cube and then fitting the inside of the O-Grid to the cube using the prescribed points of the model. The vertices of the cube were projected to the surface of the sphere. This results in fitting the cube inside of the sphere. The vertices of the blocks were aligned in all directions. O-Grid was created around the block of the cube inside of the sphere. Inflation layers had to be generated such that that the first layer height of the cell is small enough to closely and accurately capture the flow. We choose the near wall modeling of the SST k-w which requires the first cell height to be small enough such that the wall y+ is less than 1.

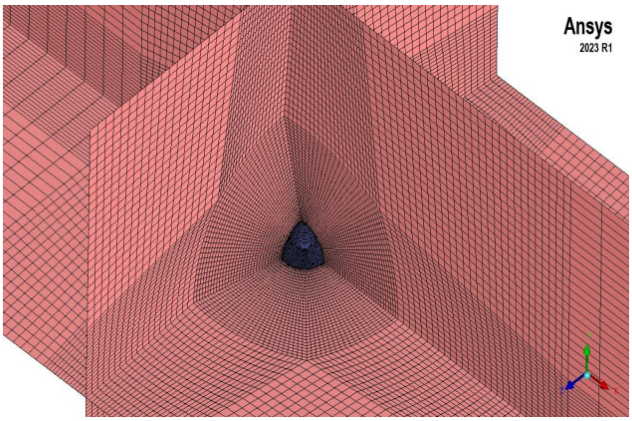

Figure 4: Isometric view of ICEM Hexa Meshing

2.3 Computational setup and boundary condition

SST k-ω was used for the calculation of drag force. The absolute convergence criteria was set as 0.001 for continuity, x-velocity, y-velocity, z-velocity, k and ω. This ensures the result is within acceptable range. No slip condition is imposed in the wall i.e. zero shear stress. Steady state model was chosen. The boundary layer of the sphere was modelled with correct value of y+. The inlet was modelled as velocity inlet and pressure outlet boundary condition was imposed in the outlet. The turbulent intensity was set to 5% [12]. Literature review had revealed that the drag coefficient will decrease rapidly with increase in the turbulent flow intensity. The reference value

was taken from the inlet with the reference area given that of the projected area of sphere. The report definition was given for the drag force of the sphere and the coefficient of drag for each value of force was calculated as,

$$C_d = \frac{2FD}{\rho u^2 A}$$

Standard initialization was done from the inlet and calculation was allowed to 10,000 iteration or convergence criteria of 0.001, which ever condition is met first.

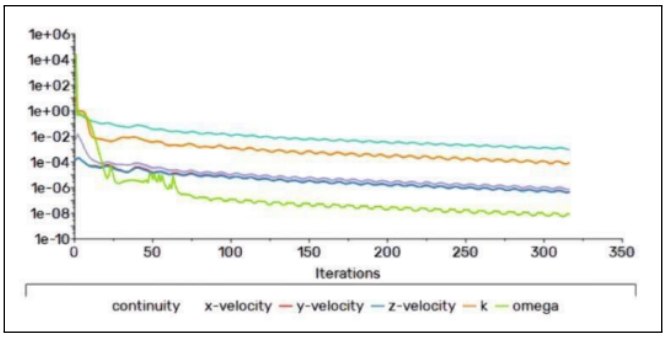

Figure 5: Residual Chart

3. Results

3.1 Mesh independent Test

It involves systematically varying the mesh size to assess the impact of mesh resolution on the simulation results. The goal is to determine the point at which further mesh refinement does not significantly alter the simulation outcome, indicating convergence and ensuring that the results are robust and reliable. The data's plotted in graph of C_d against number of mesh is shown in figure 6.

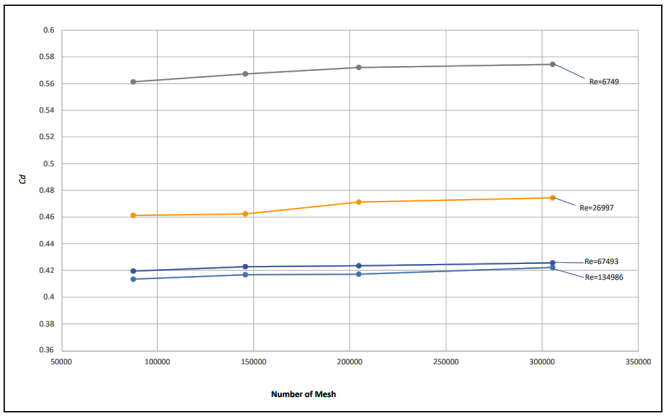

Figure 6: Mesh Independence Chart

Figure 7 shows the comparison of coefficient of drag for different values of Reynold's number at different blockage ratio. An important observation that can be made from the line chart is the graph of C_d obtained from numerical analysis at a blockage ratio of 0.3; the general trend of values of C_d is lower than the line graphs obtained at blockage of 0.5 from both numerical analysis and the experimental result of Archenbach ,1972 [3]. This result matches with the existing literature that the value of C_d is higher at a high blockage. The fact that at a high blockage ratio, the interference of boundary layer from the walls can be the result of this high value of drag. From the comparison of C_d obtained from our numerical analysis and the experiments results from Archenbach,1972 [3] done at blockage of 0.5, the minimum error percentage was 0.59% at R_e of 202550.32 and the maximum percentage of error was 18.02% at R_e of 80991.

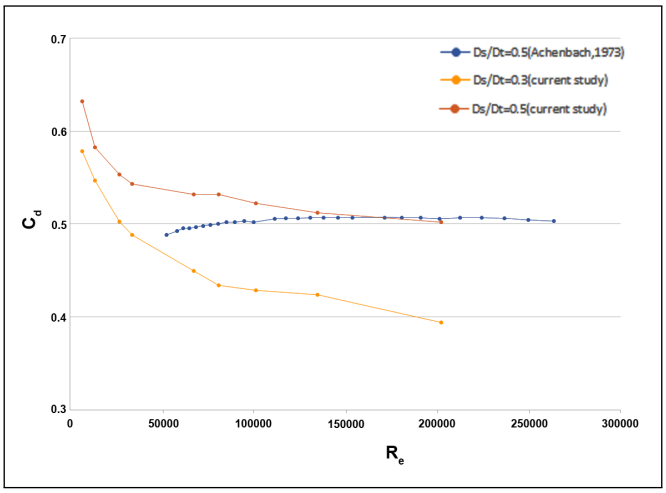

Figure 7: C_d vs R_e graph

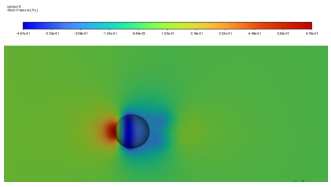

Figure 8: Static pressure contour for R_e = 12009

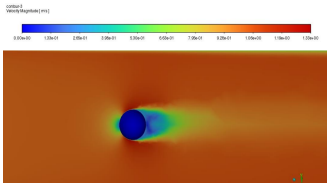

Figure 9: Velocity conotur for R_e = 12009

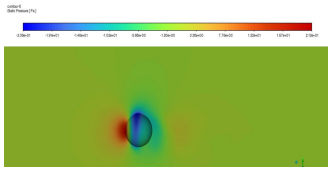

Figure 10: Static pressure contour for R_e = 90295

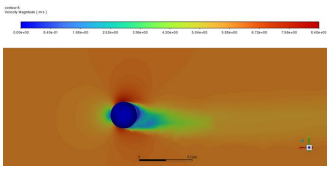

Figure 11: Velocity conotur for R_e = 90295

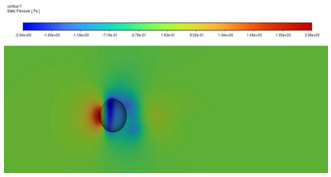

Figure 12: Static pressure contour for R_e = 21309

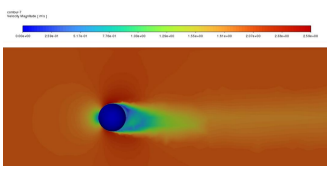

Figure 13: Velocity conotur for R_e = 21309

From the velocity contour, stagnation point can be seen at the tip of the sphere. The stagnation point (S_t) is the point on the sphere surfaces where the oncoming flow is divided either side of the sphere. Thus the velocity at the stagnation point is zero and thus the static pressure is maximum. For a laminar flow

the pressure distribution between the front and the back of the sphere is equal with the lowest pressure occurring at the pole of the sphere. The comparison of the velocity contour at various R_e reveals that the turbulent wake becomes narrower as the R_e increases. Similarly as the broadness of the turbulent wake decreases, the separation point is shifted further behind the sphere. A turbulent wake behind the sphere alters the pressure distribution, with pressures on the front of the sphere being larger than those at the back

References

[1] Edward Lewis Houghton and Peter William Carpenter. *Aerodynamics for engineering students*. Elsevier, 2003.

[2] Chang-Koon Choi and Dae-Kun Kwon. Wind tunnel blockage effects on aerodynamic behavior of bluff body. *Wind Struct Int J*, 1(4):351–364, 1998.

[3] Elmar Achenbach. Experiments on the flow past spheres at very high reynolds numbers. *Journal of fluid mechanics*, 54(3):565–575, 1972.

[4] C von Wieselsberger. Weitere feststellungen uber die gesetze des flussigkeits und luftwiderstandes (other observations on the laws of fluid and air resistance). *Physik Zeitschrift*, 23:219–224, 1922.

[5] MooreDW, PG Saffman, and T Maxworthy. The flow induced by the transverse motion of a thin disk in its own plane through a contained rapidly rotating viscous liquid. *Journal of Fluid Mechanics*, 39(4):831–847, 1969.

[6] Armin Wulf and Vedat Akdag. Tuned grid generation with icem cfd. In *Nasa conference publication*, pages 477–477. NASA, 1995.

[7] Arthur G Kravchenko and Parviz Moin. Numerical studies of flow over a circular cylinder at re d= 3900. *Physics of fluids*, 12(2):403–417, 2000.

[8] George Constantinescu and Kyle Squires. Les and des investigations of turbulent flow over a sphere. In *38th Aerospace Sciences Meeting and Exhibit*, page 540, 2000.

[9] Sadatoshi Taneda. Experimental investigation of the wake behind a sphere at low reynolds numbers. *Journal of the physical society of Japan*, 11(10):1104–1108, 1956.

[10] Ananias G Tomboulides and Steven A Orszag. Numerical investigation of transitional and weak turbulent flow past a sphere. *Journal of Fluid Mechanics*, 416:45–73, 2000.

[11] Vojtěch Spálenskỳ and Dalibor Rozehnal. Cfd simulation of dimpled sphere and its wind tunnel verification. In *MATEC Web of Conferences*, volume 107, page 00077. EDP Sciences, 2017.

[12] User Manual. Ansys fluent 12.0. *Theory Guide*, 67, 2009.